Yttrium Oxide Upconverting Phosphors. Part 4: Upconversion Luminescent Emission from Thulium-Doped Yttrium Oxide under 632.8-nm Light Excitation

J. Silver,* M. I. Martinez-Rubio, T. G. Ireland, G. R. Fern, and R. Withnall*

Centre for Phosphors and Display Materials, Chemical and Life Sciences, University of Greenwich, Chatham Maritime Campus, Chatham, Kent ME4 4TB, United Kingdom

Received: June 6, 2002; In Final Form: November 19, 2002

Strong blue upconversion emission has been observed from Y_2O_3:Tm^{3+} phosphors under 632.8-nm excitation, in addition to weaker green and red emissions. All of these emissions, including the red, showed a two-photon intensity dependence on the incident 632.8-nm laser power. The emissions that showed only a one-photon intensity dependence occurred in the near-IR region of the spectrum. The mechanism for the origins of these emissions was derived from temperature studies over the range of 0 to −190 °C and their dependence on the laser power at room temperature. Energy values are derived for all of the Tm^{3+} levels in the cubic Y_2O_3 lattice between the $^3H_6$ ground state and the $^1D_2$ excited state at ca. 27 500 cm^{-1} from the positions of the emission bands.

Introduction

We have recently reported studies on cubic Y_2O_3:Er^{3+} and Y_2O_3:Eu^{3+} lattices using 632.8-nm laser excitation.[1−3] In both materials, evidence was found for the presence of the dopant rare-earth element cation on each of the two different lattice sites. In the cubic Y_2O_3 lattice, there are two independent M^{3+} sites, one with C_2 symmetry (75% of the M^{3+} sites) and the other with S_6 symmetry (25% of the M^{3+} sites), as shown in Figure 1. In the case of Y_2O_3:Er^{3+}, the 632.8-nm excitation directly promotes the Er^{3+} ion to the $^4F_{9/2}$ state, and then the second photon promotes it to higher-lying levels.[1,2] For Y_2O_3:Eu^{3+} under 632.8-nm light excitation, the Eu^{3+} ion is promoted to the ^5D_o level; this is possible only because the $^7F_2$ sublevels are initially thermally populated, so irradiation with 632.8-nm light provides sufficient energy to span the Eu^{3+} ^7F_o $-^5D_o$ energy gap.[3]

In this work, the possibility of observing upconversion emission from cubic Y_2O_3:Tm^{3+} under 632.8-nm HeNe laser light excitation is investigated. There have been two previous studies[4,5] on Tm^{3+}-doped materials excited with red laser light, but in both cases, the materials were codoped. Cs_2NaYCl_6:Tm,Mo and Cs_2ZrCl_6:Tm,Re were excited with light of wavelengths in the range of 620−640 nm using a dye laser[4] whereas Tm^{3+},Er^{3+} codoped tellurite glasses were pumped at 650 nm to investigate the upconversion characteristics of Tm^{3+} and Er^{3+} luminescences.[5] In both of these cases, the assignments of the emissions are not in agreement with the current assignments. This is because, in the work reported herein, the component states of the ^3H term have been reassigned so that they increase in energy in the order $^3H_6$, $^3H_4$, and $^3H_5$, the last two being reversed in the previous assignments.

In addition, red-to-blue upconversion has also been observed in Y_2SiO_5:Tm^{3+} using tunable red excitation in the 640−690-nm range.[6] However, minimal assignments were undertaken in this last work, as it was noted that the internal dynamics were complicated.

* Corresponding authors. E-mail: j.silver@gre.ac.uk, r.withnall@gre.ac.uk. Fax: 44-208-331-8405.

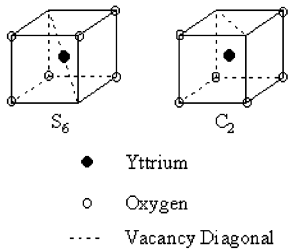

Figure 1. Two Y^{3+} crystallographic sites in cubic Y_2O_3.

Experimental Section

Chemical Preparation. The chemicals used in this study are yttrium oxide (99.99%, Rhone Poulenc, France), thulium(III) nitrate pentahydrate (99%, Aldrich), urea, and nitric acid (BDH AnalaR). The urea homogeneous precipitation method[7−14] was used to prepare spherical Y_2O_3:Tm^{3+} hydroxycarbonate submicrometer phosphor precursor powders. Yttrium nitrate stock solution (56.4 g/L) was prepared by dissolving Y_2O_3 in dilute nitric acid until the solution reached a pH of 3. Thulium nitrate (0.02 g) and urea (15.0 g) were dissolved in 500 mL of the $Y(NO_3)_3$ stock solution after it had been diluted 20-fold with deionized water. The solution was kept boiling on a hot plate until turbidity was observed, and then it was left for 1 h. The precipitates were filtered and washed twice with deionized water.

The precipitates were dried at 60 °C, giving soft, white powders that were converted to the oxide by firing at 980 °C in air for 6 h. The final ion concentration ratio, Tm^{3+}:Y^{3+}, was 1:100. All of the powders consisted of Y_2O_3 in the cubic phase, as was made evident by X-ray powder diffraction data.[1]

Characterization of Physical Properties. The morphologies and the particle sizes of the samples were determined by scanning electron microscopy (SEM) using a Cambridge Instruments Stereoscan 90 and transmission electron microscopy (TEM) using a JEOL JEM-200CX. The average diameter of the spherical particles was estimated to be 300 ± 50 nm from the measurement of ∼50 particles per SEM picture.

10.1021/jp021372s CCC: $25.00
Published on Web 01/28/2003

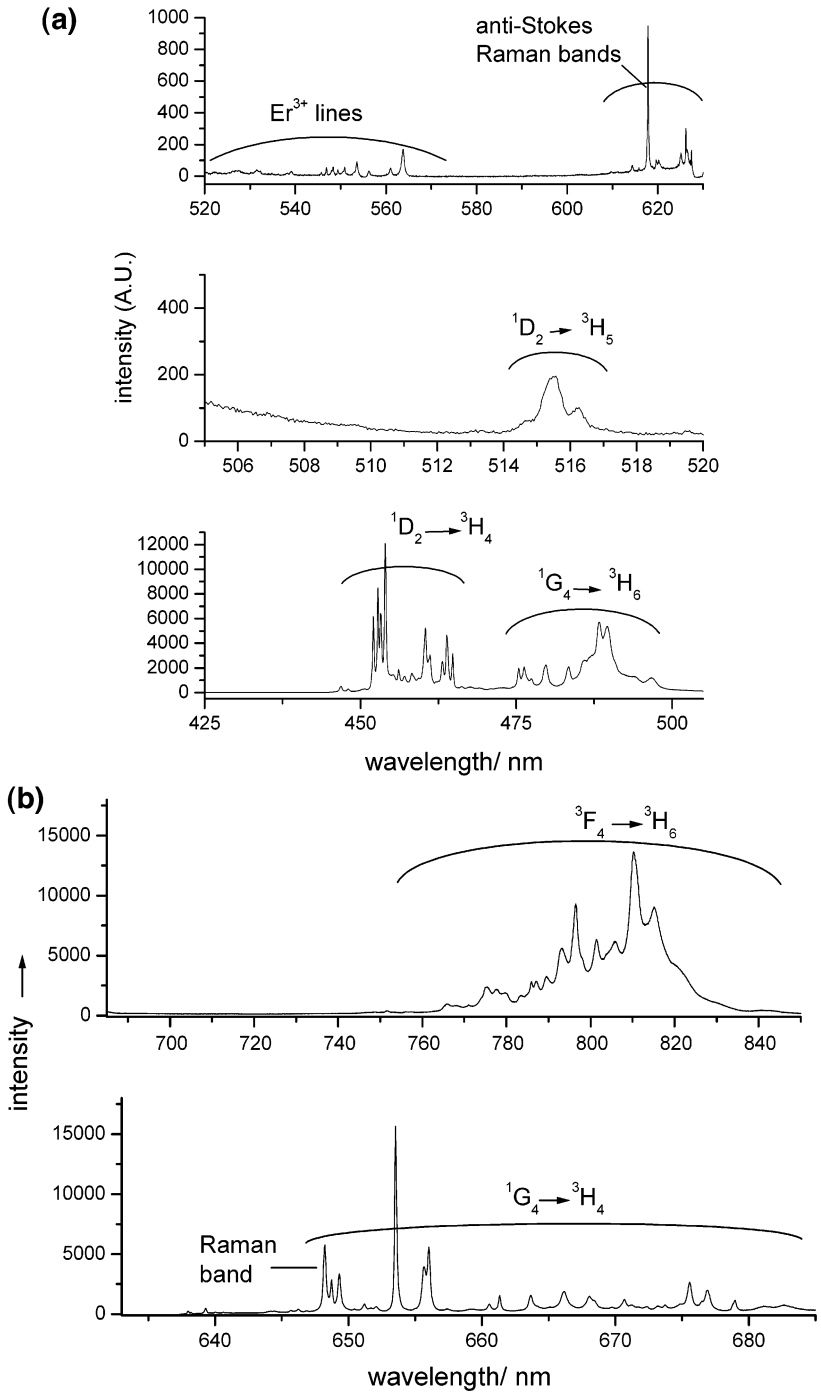

Figure 2. (a) Anti-Stokes emission spectrum at 25 °C of particles of Y_2O_3:Tm^{3+} fired at 980 °C for 6 h. (b) Stokes emission spectrum at 25 °C of particles of Y_2O_3:Tm^{3+} fired at 980 °C for 6 h.

Luminescence and Raman spectra were obtained using a Labram Raman spectrometer equipped with 1800 and 600 grooves/mm holographic gratings, a holographic supernotch filter, and a peltier-cooled CCD detector. Samples were excited at a wavelength of 632.8 nm using a HeNe laser with an output of 8 mW of power at the sample, unless an attenuation filter was used. Precise control of the sample temperature (±0.1 °C) was achieved by means of a Linkam THMS600 temperature-programmable heating/cooling microscope stage. For cooling, the THMS stage was used in conjunction with a Linkam LNP cooling system.

Spectral intensities were normalized using the Stokes Raman band at 375 cm^{-1} of cubic Y_2O_3.

Results and Discussion

All of the Y_2O_3:Tm^{3+} samples were shown to have crystallized in the cubic phase from their X-ray diffraction patterns. TEM and SEM images of typical samples can be seen in Figures 1S and 2S, respectively, of the Supporting Information. From the examples shown in these Figures, the samples used for this work can be seen to be made up of hollow spheres. Such hollow spheres are not uncommon, and we have previously noted similar ones for Y_2O_3:Eu^{3+}.[14,15]

The emission spectrum of cubic Y_2O_3:Tm^{3+} at 25 °C is presented in Figure 2. The electronic energy levels of Y_2O_3:Tm^{3+} in the 0−30 000-cm^{-1} region are shown in Figure 9 of

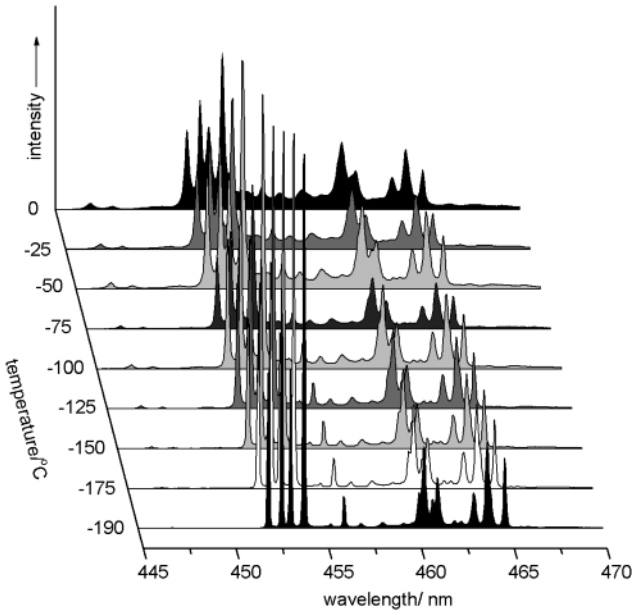

Figure 3. Emission bands of Tm^{3+} in Y_2O_3 in the 445- to 470-nm region. The spectra are shown in the order of increasing temperature from bottom to top: −190, −175, −150, −125, −100, −75, −50, −25, and 0 °C.

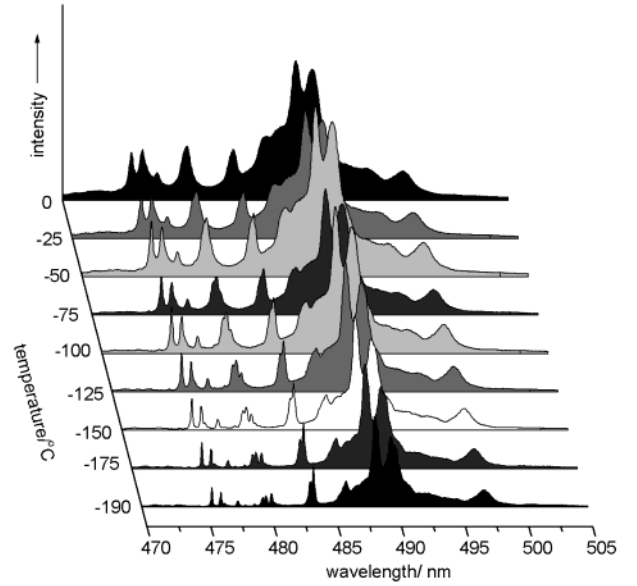

Figure 4. Emission bands of Tm^{3+} in Y_2O_3 in the 470- to 505-nm region. The spectra are shown in the order of increasing temperature from bottom to top: −190, −175, −150, −125, −100, −75, −50, −25, and 0 °C.

this article, and all possible transitions between them are listed and assigned to observed emission features, where observed, in Table 1. When Y_2O_3:Tm^{3+} is excited by 632.8-nm radiation, the main emission features observed over the range of 400−875-nm are due to the following transitions: $^1D_2 \rightarrow {}^3H_4$, $^1D_2 \rightarrow {}^3H_5$, $^1G_4 \rightarrow {}^3H_6$, $^1G_4 \rightarrow {}^3H_4$, and $^3F_4 \rightarrow {}^3H_6$.

Stark sublevels of the ground and low-lying excited states of Tm^{3+} ions on the C_2 sites of cubic Y_2O_3 have been previously assigned.[16] The energy of the 632.8-nm excitation falls outside the energy range of the $^3H_6 \rightarrow {}^3F_2$ transition that was previously reported.[16] Because phonon coupling of the lattice to the rare-earth cations on both extremities of the lanthanide series is known to be important, it is likely that the absorption of one photon of the 632.8-nm laser light promoted the Tm^{3+} ion from the $^3H_6$ ground level to a phonon-coupled level of the $^3F_2$ excited state. The phonon energies of the Y_2O_3 lattice are in the range of 0−600 cm^{-1}, where bands due to fundamental vibrations are observed in the Raman spectrum of this lattice.[1−3]

TABLE 1: Possible Electronic Transitions for Emission from the Y_2O_3:Tm^{3+} Phosphor Absorbing a Maximum of Two 632.8-nm Photons

transition	wavelength	photon dependence
$^1D_2 \rightarrow {}^3H_6$[a]		
$^1D_2 \rightarrow {}^3H_4$	450−470 nm	2
$^1D_2 \rightarrow {}^3H_5$	512−517 nm	2
$^1D_2 \rightarrow {}^3F_4$	not observed	
$^1D_2 \rightarrow {}^3F_3$	small features possibly observed (see text)	2
$^1D_2 \rightarrow {}^3F_2$	not observed	
$^1D_2 \rightarrow {}^1G_4$[a]		
$^1G_4 \rightarrow {}^3H_6$	475−498 nm	2
$^1G_4 \rightarrow {}^3H_4$	648−687 nm	2
$^1G_4 \rightarrow {}^3H_5$	small features possibly observed (see text)	2
$^1G_4 \rightarrow {}^3F_4$	not observed	
$^1G_4 \rightarrow {}^3F_3$[a]		
$^1G_4 \rightarrow {}^3F_2$[a]		
$^3F_2 \rightarrow {}^3H_6$	not observed	
$^3F_2 \rightarrow {}^3H_4$	1079−1127 nm	1
$^3F_2 \rightarrow {}^3H_5$	not observed	
$^3F_2 \rightarrow {}^3F_4$[a]		
$^3F_2 \rightarrow {}^3F_3$[a]		
$^3F_3 \rightarrow {}^3H_6$	not observed	
$^3F_3 \rightarrow {}^3H_4$[a]		
$^3F_3 \rightarrow {}^3H_5$[a]		
$^3F_3 \rightarrow {}^3F_4$[a]		
$^3F_4 \rightarrow {}^3H_6$	762−836 nm	1
$^3F_4 \rightarrow {}^3H_4$[a]		
$^3F_4 \rightarrow {}^3H_5$[a]		
$^3H_5 \rightarrow {}^3H_6$	not observed	
$^3H_5 \rightarrow {}^3H_4$[a]		
$^3H_4 \rightarrow {}^3H_6$[a]		

[a] Beyond our detection range.

From the assignments in Table 1, the occupation of the $^1D_2$ level necessitates a two-photon process that occurs in two steps. This process involves an energy decay of the Tm^{3+} ion from the $^3F_2$ level to a lower level before the absorption of a second photon of 632.8-nm light can promote it to the $^1D_2$ level (see the schematic energy-level diagram for Y_2O_3:Tm^{3+} in Figure 9 of this article). From the energy-level diagram for Y_2O_3:Tm^{3+} (see later), it can be seen that the $^1D_2-{}^3F_4$ energy gap of the Tm^{3+} ion closely matches the energy of a photon of 632.8-nm light. Thus, the Tm^{3+} ion has to decay from the $^3F_2$ level to the $^3F_4$ level before a second photon is absorbed, promoting the ion to the $^1D_2$ level.

From the $^1D_2$ level, the Tm^{3+} ion can decay radiatively via the $^1D_2 \rightarrow {}^3H_4$ transition, which gives rise to a strong blue emission, or via the $^1D_2 \rightarrow {}^3H_5$ transition, which gives rise to a weak green emission (see Figure 2a). Radiative decay via the $^1D_2 \rightarrow {}^3H_6$ transition could also occur, but this would give rise to an emission in the near-UV region at ca. 28 000 cm^{-1}, which was not observed. Another decay pathway from the $^1D_2$ level occurs via relaxation to the $^1G_4$ level. Subsequent decay from the $^1G_4$ level takes place by radiative decays back to the $^3H_6$ ground level, giving rise to a second strong, blue emission (see Figure 2a), and to the $^3H_4$ level, giving a strong, red emission (see Figure 2b). There is no evidence for radiative decay via the $^1D_2 \rightarrow {}^3F_2$ and $^1D_2 \rightarrow {}^3F_4$ transitions, but we cannot rule out the possibility that weak emission features in the red region are due to the $^1D_2 \rightarrow {}^3F_3$ transition (see later). A further strong emission, not yet mentioned, occurs in the red region, and this is assigned to the $^3F_4 \rightarrow {}^3H_6$ transition (see Figure 2b). In

addition, very weak features observed between 1079 and 1127 nm are assigned to the $^3F_2 \rightarrow {}^3H_4$ transition. The assignments of the present work are given in Table 1 and Figure 9 of this article.

The two-photon process explains how the $^1D_2$ and $^1G_4$ levels are populated. The population of the lower energy levels can be explained by a one-photon process.

Thus, the anti-Stokes emission from cubic Y_2O_3:Tm^{3+} under 632.8-nm excitation involves a decay by ca. 2500 cm^{-1} of the Tm^{3+} ion down to the $^3F_4$ state, after initial excitation to the $^3F_2$ state, before the absorption of a second photon of 632.8-nm light. This two-photon absorption mechanism, which results in anti-Stokes emission, is different from those occurring when cubic Y_2O_3:Er^{3+} and cubic Y_2O_3:Eu^{3+} are excited by 632.8-nm light because the Er^{3+} and Eu^{3+} ions do not decay from their initially excited states before the absorption of a second photon.[1−3] This would be reflected in the time evolution of these signals, which is beyond the scope of the present work.

To make the assignments of the emission bands shown in Figure 2, the emission spectra were studied over the temperature range of 0 to −190 °C, and the laser power dependence of the band intensities was investigated.

Temperature Dependence of Emission Peaks (0 to −190 °C). In Figure 3, the temperature dependence of the $^1D_2 \rightarrow {}^3H_4$ transition is shown from 0 to −190 °C. It is apparent that the three small bands at 446.8, 448, and 450.5 nm (see Figure 3) that disappear at −190 °C are clearly behaving differently from the four bands above 451 nm, at 452.1, 452.6, 453.1, and 453.9 nm, which increase in intensity as the temperature is lowered to −190 °C. The obvious explanation is that the three small bands are hot bands originating from thermal population of higher-energy Stark sublevels of the $^1D_2$ state, which has $2J + 1 = 5$ components, and this thermal population decreases as the temperature drops. All of the other bands in Figure 3 behave identically, in keeping with them all arising from the $^1D_2 \rightarrow {}^3H_4$ transition.

The emission bands observed between 474 and 500 nm are presented in Figure 4. The bands in the range of 475−485 nm sharpen considerably, and that at 480 nm splits on going down in temperature, but the other bands in the 485−500-nm range do not split and show very little sharpening. The only transition that can possibly explain these two groups of bands is the $^1G_4 \rightarrow {}^3H_6$ transition. At −190 °C, two of the bands not only have narrowed but also have split into a number of components. These are the bands around 480 nm (four bands at −190 °C but only one band at 0 °C) and that at 483 nm (which is a doublet at −190 °C and almost a singlet at 0 °C). The most likely explanation for these observations is a change in the Maxwell−Boltzmann distribution of populations of the Stark sublevels as the temperature decreases. There is a small triplet at 515.5 nm at 0 °C that sharpens to five bands (514.4, 514.6, 515.4, 515.6, and 516.3 nm) at −190 °C (see Figure 3S of Supporting Information). This group of bands has a different temperature dependence than the group of bands between 474 and 500 nm because the former is still increasing in intensity as the temperature is lowered toward −190 °C whereas the latter has maximum intensity at −50 °C (see Figure 4). This triplet is assigned to the $^1D_2 \rightarrow {}^3H_5$ transition. In addition, there is a sixth band around 513 nm, which is apparent at the lower temperatures and is also assigned to this transition. Again, the most likely explanation for these observations is a change in the relative populations of the Stark sublevels as the temperature decreases.

All of the other features between 517 nm and the laser line on the anti-Stokes side are anti-Stokes Raman bands.[1] On the Stokes side, the Raman bands for the Y_2O_3 lattice have been discussed previously.[1]

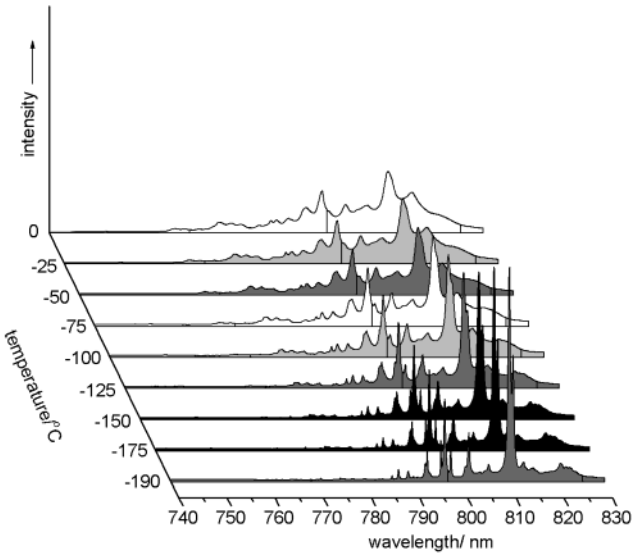

Figure 5. Emission bands of Tm^{3+} in Y_2O_3 in the 740- to 830-nm region. The spectra are shown in the order of increasing temperature from bottom to top: −190, −175, −150, −125, −100, −75, −50, −25, and 0 °C.

The bands starting at 648.5 nm and extending to 683 nm (see Figures 4S and 5S in Supporting Information) show three main types of temperature behavior between 0 and −190 °C. Those at 648.7, 649.3, 650.5, 651.2, 652.1, 654.8, 662.8, 663.7, 669.3, and 673 nm are most intense at 0 °C and least intense at −190 °C except for the last of these bands (673 nm), which also shows some intensity at −125 °C. The bands at 653.6, 656.2, and 660.6, the five spanning 671 to 672.5, and all of those from 673.6 to 683 nm are maximized at −125 °C. The bands at 661.6 and 665.1 nm are still increasing in intensity as the temperature is lowered toward −190 °C. The bands are assigned to the $^1G_4 \rightarrow {}^3H_4$ transition (see Figure 2b). The temperature dependence of these bands is dependent on the relative populations of the Stark sublevels of the $^1G_4$ state from where the emissions arise.

The final envelope of emission bands is shown in Figure 5. Two different temperature dependencies are seen for these bands. One subset sharpens as the temperature approaches −190 °C whereas the other almost disappears at −190 °C. In Figure 5, it is apparent that all of the features from 765 to 825 nm sharpen as the temperature decreases, and in several cases, the intensities of the emission bands are much higher at −190 °C than at 0 °C. In the 745- to 765-nm region, the opposite behavior is apparent because the intensities of the bands decrease as the temperature decreases (particularly that at 750.4 nm). In this case, the different thermal behavior is due to the fact that there are two different transitions that give rise to the emission bands in this region. The main transition is $^3F_4 \rightarrow {}^3H_6$, and a second transition accounts for the bands between 745 and 760 nm and is discussed in Laser Power Dependence (see below).

There was no indication in this study for different temperature behavior of the Tm^{3+} ions on the C_2 and S_6 crystallographic sites of the cubic Y_2O_3 lattice; therefore, it is not possible to identify Stark levels of Tm^{3+} ions on either site. However, there is a higher probability that the cations are located on the C_2 sites because there are 3 times as many as the S_6 sites.

The concentration of Tm^{3+} ions is 1:100 of the total cations. Because the phosphor material was prepared by homogeneous precipitation, it is reasonable to assume that clustering of Tm^{3+} ions has not occurred. It would therefore be reasonable to expect

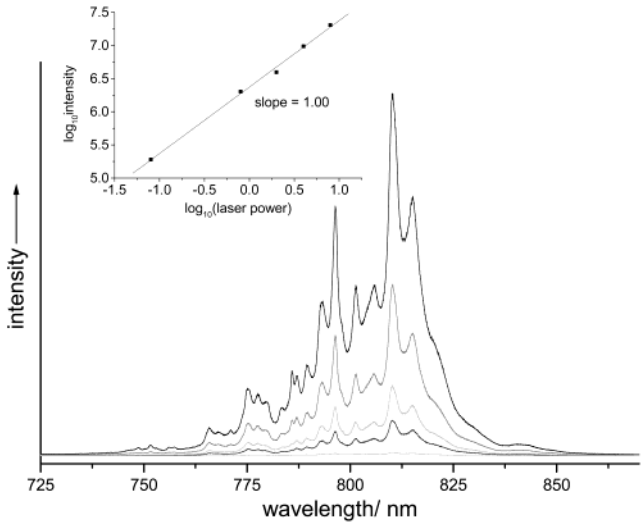

Figure 6. Power dependence of the near-IR emission bands in the 725- to 855-nm region. The spectra are shown in the order of increasing laser exciting power from bottom to top: 0.08, 0.8, 2, 4, and 8 mW. The insert shows a logarithmic plot of emission intensity vs laser power showing a one-photon dependence of this emission.

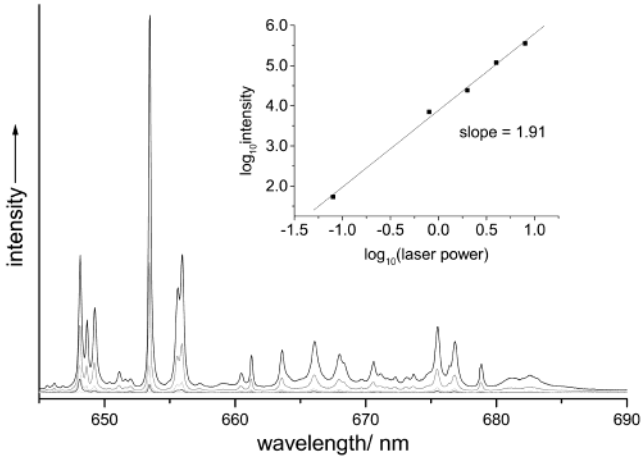

Figure 7. Power dependence of the red emission bands in the 645- to 690-nm region. The spectra are shown in the order of increasing laser exciting power from bottom to top: 0.08, 0.8, 2, 4, and 8 mW. The insert shows a logarithmic plot of emission intensity vs laser power showing a two-photon dependence of this emission.

each Tm^{3+} ion to be separated from its nearest Tm^{3+} neighbor by over 8 Å, and hence the Tm^{3+} concentration is at the single-ion level.

Laser Power Dependence. Stokes Emission Bands. Figure 6 presents the laser power experimental data for the region 760−840 nm. The inset, which is a logarithmic plot of laser power versus emission intensity having a slope of 1.0, shows that most of these features in this spectral region are due to a one-photon process. From the energy range of this transition, we assign it to the $^3F_4 \rightarrow {}^3H_6$ transition. As the laser photon has a closer energy match to the $^3F_2-{}^3H_6$ energy gap, nonradiative decay from the $^3F_2$ to the $^3F_4$ level must then occur. Because no other bands in the spectra show a one-photon dependence, we can eliminate the $^3F_3-{}^3H_6$ and the $^3F_2-{}^3H_6$ from occurring under red laser excitation.

Figure 6 also shows some very small features in the region 745.5 to 768.6 nm, a small band at 771.0 nm, and a band at 785.9 nm that have a photon dependence greater than 1 (see Figure 6S in Supporting Information). These bands either arise from the $^1D_2 \rightarrow {}^3F_3$ transition or the $^1G_4 \rightarrow {}^3H_5$ transition or both. There is no evidence for the presence of a $^1D_2 \rightarrow {}^3F_2$ transition.

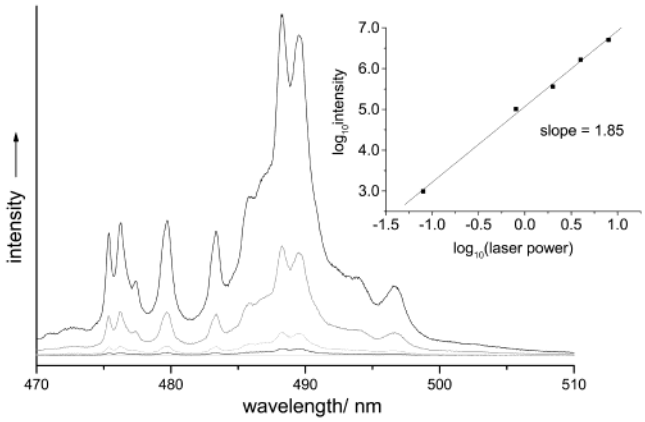

Figure 8. Power dependence of the blue emission bands in the 470- to 510-nm region. The spectra are shown in the order of increasing laser exciting power from bottom to top: 0.08, 0.8, 2, 4, and 8 mW. The insert shows a logarithmic plot of emission intensity vs laser power showing a two-photon dependence of this emission.

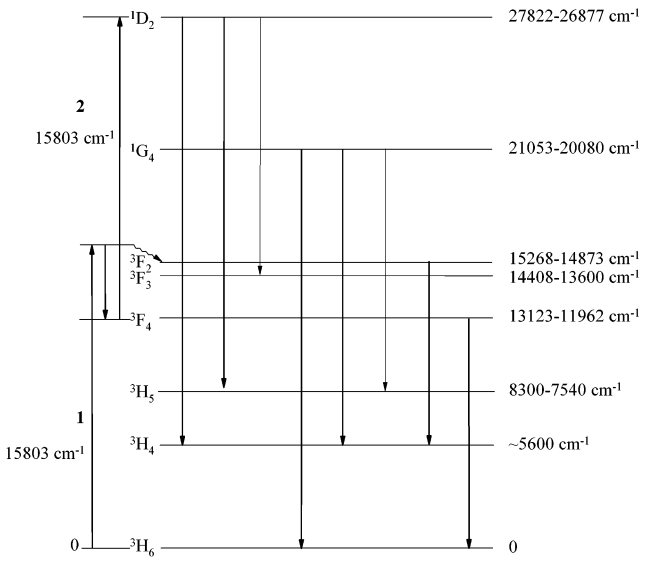

Figure 9. Schematic energy-level diagram for Tm^{3+} ions in cubic Y_2O_3. The values of the energies of the levels above the ground state are derived in this work.

For the emission bands above the Stokes Raman band at 375 cm^{-1} (648 nm) to 679 nm (see Figure 7), the photon dependence was determined by plotting the intensity of the peak at 653.5 nm (see the inset of Figure 7, which indicates a two-photon dependence). Because there is no two-photon dependence of the $^3F_4 \rightarrow {}^3H_6$ transition, the $^1D_2 \rightarrow {}^3F_4$ transition can be eliminated, leaving the $^1G_4 \rightarrow {}^3H_4$ transition as the only possible transition to which this band can be assigned.

Anti-Stokes Emission Bands. Figure 8 presents the 470- to 510-nm anti-Stokes region. The inset, which is a logarithmic plot of laser power versus emission intensity, shows that this transition is due to a two-photon process. This is consistent with a $^1G_4 \rightarrow {}^3H_6$ transition. For this transition to occur, the $^1D_2 \rightarrow {}^1G_4$ transition must occur first, although this is outside the detection range of the Raman spectrometer used in this study.

The anti-Stokes emission bands in the 445- to 470-nm region are given in Figure 7S in Supporting Information. In the inset to Figure 7S, it is apparent that the slope indicates a two-photon dependence, and these wavelengths are consistent with a $^1D_2 \rightarrow {}^3H_4$ transition.

The $^1G_4 \rightarrow {}^3H_6$ transition is approximately equal in intensity to the $^1D_2 \rightarrow {}^3H_4$ transition.

The small features between 1079 and 1127 nm due to the $^3F_2 \rightarrow {}^3H_4$ transition showed a one-photon dependence.

In Figure 9, we present the overall energy-level diagram for Y_2O_3: Tm^{3+}, which shows the transitions giving rise to the emission bands that we have observed when using 632.8-nm excitation. The values of the energies of the levels above the ground state shown in Figure 9 are derived from the spectra reported in this work. These values do not take account of the spread of the energies in the $^3H_6$ ground state arising from Stark split levels and the coupling of lattice phonons to these levels. However, when considering the values quoted in a previous report for the $^3H_6 \rightarrow {}^3F_2$ transition[16] (which show very good agreement with our results), the initial excitation by one photon of 632.8-nm light (15 803 cm^{-1}) would promote the Tm^{3+} ion to a level that is no more than one phonon of $\sim$600 cm^{-1} magnitude away from the $^3F_2$ state. We might well expect the other transitions to be affected to a similar extent by phonon coupling of the lattice to the rare-earth cations.

Conclusions

It is demonstrated herein that when cubic Y_2O_3: Tm^{3+} is excited by 632.8-nm red laser light the incoming photon effects a transition to the $^3F_2$ level of the Tm^{3+} ion. This excited ion relaxes to the $^3F_4$ level, from where it returns to the $^3H_6$ ground state producing 762−836-nm emission unless a second incident 632.8-nm photon is absorbed by the excited Tm^{3+} ion. The second photon excites the Tm^{3+} ion to the $^1D_2$ level. From this level, all of the observed emissions (see Table 1 and Figure 9) showing a two-photon dependence originate either directly or indirectly after relaxation to the $^1G_4$ level. Among these, there are two intense emissions due to the $^1D_2 \rightarrow {}^3H_4$ and $^1G_4 \rightarrow {}^3H_6$ transitions in the blue region of the spectrum and, surprisingly, a red emission due to the $^1G_4 \rightarrow {}^3H_4$ transition at lower energy than that of the exciting 632.8-nm photons.

There was no observable discrimination between emissions from Tm^{3+} ions on C_2 and S_6 sites of the Y_2O_3 lattice.

The temperature dependence of the spectra can be largely explained by the effects of phonon coupling of the lattice to the rare-earth cations.

Acknowledgment. We express our gratitude to the EPSRC (grant ref nos. GR/L85176, GR/M78847, and GR/N28535).

Supporting Information Available: TEM and SEM micrographs of particles of Y_2O_3: Tm^{3+} after firing at 980 °C in air for 6 h. Emission bands of Tm^{3+} in Y_2O_3 in the 510- to 520-nm, 645- to 660-nm, and 660- to 685-nm regions Power dependence of near-IR emission in the 740- to 790-nm region. This information is available free of charge via the Internet at http://pubs.acs.org.

References and Notes

(1) Silver, J.; Martinez-Rubio, M. I.; Ireland, T. G.; Fern, G. R.; Withnall, R. *J. Phys. Chem. B* **2001**, *105*, 948.
(2) Silver, J.; Martinez-Rubio, M. I.; Ireland, T. G.; Withnall, R., *J. Phys. Chem. B* **2001,** *105*, 7200.
(3) Silver, J.; Martinez-Rubio, M. I.; Ireland, T. G.; Fern, G. R.; Withnall, R. *J. Phys. Chem. B* **2001**, *105*, 9107.
(4) Kirk, A. D.; Furer, N.; Güdel, H. U. *J. Lumin.* **1996**, *68*, 77.
(5) Tanabe, S.; Suzuki, K.; Soga, N.; Hanada, T. *J. Lumin.* **1995**, *65*, 247.
(6) Bielejec, E.; Kisel, E.; Silversmith, A. *J. Lumin.* **1997**, *72*−*74*, 62.
(7) Sordelet, D.; Akinc, M. *J. Colloid Interface Sci.* **1988**, *122*, 47.
(8) Milosevic, O.; Jordovic, B.; Uskokovic, D. *Mater. Lett.* **1994**, *19*, 165.
(9) Kim, M. J.; Matijevic, E. *J. Mater. Res.* **1991**, *6*, 840.
(10) Giesche, H.; Matijevic, E. *J. Mater. Res.* **1994**, *9*, 436.
(11) Nishisu, Y.; Kobayashi, M. U.S. Patent 5,413,736, 1995.
(12) Pei, Y.; Liu, X. *Chin. J. Lumin.* **1996**, *17*, 5.
(13) Jiang, Y. D.; Wang, Z. L.; Zhang, F.; Paris, H. G.; Summers, C. J. *J. Mater. Res.* **1998**, *13*, 2950.
(14) Vecht, A.; Gibbons, C.; Davies, D.; Jing, X.; Marsh, P.; Ireland, T. G.; Silver, J.; Newport, A. *J. Vac. Sci. Technol., B* **1999**, *17*, 750.
(15) Jing, X.; Ireland, T. G.; Gibbons, C.; Barber, D. J.; Silver, J.; Vecht, A.; Fern, G.; Trogwa, P.; Morton, D. *J. Electrochem. Soc.* **1999**, *146*, 4564.
(16) Leavitt, R. P.; Gruber, J. B.; Chang, N. C.; Morrison, C. A. *J. Chem. Phys.* **1982**, *76*, 4775.